RSC Sustainability

ROYAL SOCIETY OF CHEMISTRY

PAPER

View Article Online
View Journal | View Issue

Cite this: *RSC Sustainability*, 2026, **4**, 279

Ionic and non-ionic organic porous adsorbents for the removal of chloramphenicol and ciprofloxacin from water†

Sunny K. S. Freitas,[ab] Letícia R. C. Correa,[a] Verônica D. da Silva,[b] Pierre M. Esteves *[a] and Luis C. Branco *[b]

Nanoporous organic materials with varying pore sizes were utilized to remove antibiotics from surface and groundwater. These adsorbents belong to the group of Covalent Organic Frameworks (COFs), known for their high stability, porosity, and large surface area. Given their characteristics, which are well-suited for adsorption applications, these materials demonstrated relatively high capture capacities for emerging organic pollutants such as chloramphenicol (182 mg g^{-1} for **RIO-55**) and ciprofloxacin (79 mg g^{-1} for **RIO-55**) compared to other organic porous adsorbents. To conduct a comparative study on adsorption efficiency, both ionic and non-ionic materials were selected. Some ionic materials exhibited greater affinity for pharmaceutical compounds due to different adsorption mechanisms. Additionally, tests using a real water sample from the Tagus River confirmed the materials' removal efficiency. A correlation was observed between the maximum adsorption capacity and the pore width of the COFs, suggesting that better fitting of these adsorbates into mesopores enhances adsorption performance.

Received 17th March 2025
Accepted 23rd March 2025

DOI: 10.1039/d5su00198f

rsc.li/rscsus

Sustainability spotlight

Access to safe water is one of the most basic human needs for health and well-being. Considering the fast population growth and the increased water needs of agriculture, industry, and energy sectors, it is crucial to discover sustainable processes for water purification. The development of new technologies using nanoporous materials seems to be efficient to remove pharmaceutical micropollutants from water streams.

Introduction

The treatment of wastewater from industries or domestic consumption has been increasingly studied to improve the techniques and methodologies used, achieving greater efficiency.[1] The growing number of organic pollutants found in water samples from rivers, lakes, and oceans, among others, is worrying, since persistent pollutants have been increasing over time, already known by industries, environmental networks, and researchers. Additionally, there are now new risks associated with the so-called emerging pollutants,[2] including active pharmaceutical ingredients (APIs). About 50% to 90% of an API dosage is discharged unchanged to nature and these compounds persist in the environment.[3,4]

Of the persistent drugs, antibiotics are a class of greatest concern among environmentalists.[5] This is the largest category of drugs provided by human and veterinary medicine, with therapeutic purposes or as growth promoters. The increase in the consumption of antibiotics consequently generates greater disposal in the environment. Because of their use in fish culture, some antibiotics such as chloramphenicol are found in sediments of marine origin.[6] Several antibiotics can be found in wastewater due to inadequate disposal of unused drugs or their incomplete metabolism in humans.[7]

The removal efficiency of these organic pollutants in water and sewage treatment plants is minimal. This is because conventional treatment technologies have limitations in removing a variety of APIs.[8–10] Thus, new approaches involving liquid–liquid extractions, adsorption, and membrane technology have been reported to remove these and other pollutants from water. In recent years, conventional porous materials such as activated carbons and bioceramics have been mainly tested as adsorbents for water treatment processes.[11,12] However, they cannot capture many of the organic pollutants and heavy metals that may exist in the water to be treated.[13,14] An emerging class of organic nanoporous materials called Covalent Organic Frameworks (COFs) have shown to be good candidates for

[a]*Instituto de Química, UFRJ, Avenida Athos da Silveira Ramos, nº 149, Bloco A—7º andar Centro de Tecnologia—Cidade Universitária, Ilha do Fundão, Rio de Janeiro 21941-909, Brazil. E-mail: pesteves@iq.ufrj.br*

[b]*LAQV-REQUIMTE, Department of Chemistry, NOVA School of Science and Technology, NOVA University of Lisbon, Campus de Caparica, 2829-516 Caparica, Portugal. E-mail: l.branco@fct.unl.pt*

† Electronic supplementary information (ESI) available. See DOI: https://doi.org/10.1039/d5su00198f

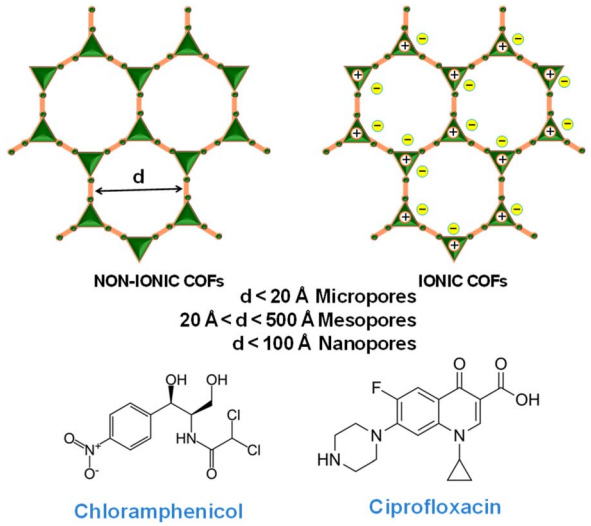

Fig. 1 The structure of a non-ionic and an ionic COF (top), the definition of porosity (middle), and the chemical structures of chloramphenicol (CLO) and ciprofloxacin (CIP).

capturing gases, ions, molecules, and biomolecules.[15–21] Hence, this class of porous materials has been selected as organic adsorbents, as they are thermally stable and possess high porosity and high specific area values. These materials are formed by light elements having different classifications according to their structure and physicochemical properties. In general, COFs can be two- or three-dimensional, ionic, or non-ionic and their synthesis can be adjusted according to the purpose of the material, forming a highly insoluble powder. They have been used for a variety of applications, especially for energy fields and environmental problems.[22–24]

Herein, selected nanoporous organic materials previously prepared by our group[15,25,26] called RIOs (acronym for Reticular Innovative Organic materials, Fig. 2), which can be non-ionic (**RIO-12**, **RIO-13**, and **RIO-24**) and ionic (**RIO-55** and **RIO-70**), are evaluated as adsorbents of ciprofloxacin and chloramphenicol antibiotics from water. The micro- and mesoporous structures of RIOs are selected to assess the effect of pore size and nature in adsorption processes.

Experimental

Synthesis and characterization of RIOs

RIO-12, **RIO-13**, **RIO-55**, and **RIO-70** were synthesized as reported in previous studies.[15,26,27] On the other hand, **RIO-24**, to our knowledge, was never previously reported. **RIO-24** was synthesized by solvothermal synthesis, where melamine (110 mg, 0.87 mmol) was added to triformylphloroglucinol (250 mg, 1.2 mmol). The solid mixture was transferred to a 48 mL high-pressure vessel (ChemGlass) and then DMSO (15 mL) and then HOAc 3 M (3 mL) were sequentially added. The reactor was closed and remained under stirring and heating (190 °C) for 3 days, resulting in a dark red powder. All detailed synthesis and physicochemical characterization of **RIO-24** are included in the ESI.†

The adsorbents were characterized as previously reported. The analysis of textural properties (isotherms and pore size distribution) is conducted on ESI. **RIO-24** was characterized by FTIR, CP-MAS ^{13}C NMR, PXRD, and N_2 adsorption and desorption.

Thermodynamic studies of adsorption

To study the adsorption of organic pollutants in water, the nanostructured porous materials were used as adsorbents and the antibiotics chloramphenicol (CLO) and ciprofloxacin (CIP) were used as adsorbates (Fig. 1). Aiming to relate the structure properties of these materials with their adsorption capacity, ionic and non-ionic adsorbents and micro- and mesoporous materials have been selected. Fig. 2 illustrates the comparative structure of the selected ionic dye-based (**RIO-55** and **RIO-70**), melamine-based (**RIO-24**), and hydrazine-based (**RIO-12** and **RIO-13**) materials.

Solutions of chloramphenicol and ciprofloxacin from commercial sources (Alfa Aesar <98% and TCI <98%, respectively) were prepared in different concentrations (5–80 ppm and 4–22 ppm, respectively). Each solution was previously analysed by UV-vis (200–500 nm) to obtain the absorbance data, where λ_{max}(chloramphenicol) = 272 nm and λ_{max}(ciprofloxacin) = 278 nm. The absorbance data were plotted *versus* concentrations, obtaining a straight line (calibration curve), whose equation allows for correction of the final values of concentration and absorbance (Fig. S13†). Then, 4 mg of adsorbent was added to 4 mL of each sample, which was placed in a shaker (2400 rpm) for 4 h and 24 h to observe the different values of adsorption. After this, the samples were filtered in specific filter papers (glass microfibre, 55 mm, Filter Lab for CIP; qualitative filter paper, 1300/80, 70 mm, Filter Lab for CLO) for each drug, previously tested to check any influence of paper on absorbance. After the filtration, the adsorbent remained on the filter paper, while the resulting solution was taken for UV-vis analysis (200–500 nm), obtaining the final values of absorbance. The method chosen to quantify the adsorption capacity involves the difference in the concentration (initial *vs.* final).

Effect of pH on the adsorption

The capture of these antibiotics in a wide pH range is highly desirable for practical waste disposal. Thus, isothermal adsorption curves at different pH values (1.5–12.5) for **RIO-70** and **RIO-24** were obtained. These RIOs were chosen to compare the pore size and adsorption capacity. In general, 4 mg of adsorbent was added to a solution of 4 mL containing the micropollutant (50 ppm for CLO and 10 ppm for CIP). The pH adjustments were performed using a corresponding solution of HCl or NaOH (0.1 M). The samples were left in a shaker for 10 min and then filtered and analysed by UV-vis. Then, the pH of the solutions was measured.

Regeneration cycles

Aiming to obtain information about the reuse of these materials after the first adsorption (**RIO-70** and **RIO-24**), regeneration tests have been performed. For these studies, 10 mg of adsorbent was added to 10 mL of pollutant solutions. For chloramphenicol, the 50 ppm solution was used while for ciprofloxacin only 10 ppm was selected. The samples were left in a shaker for

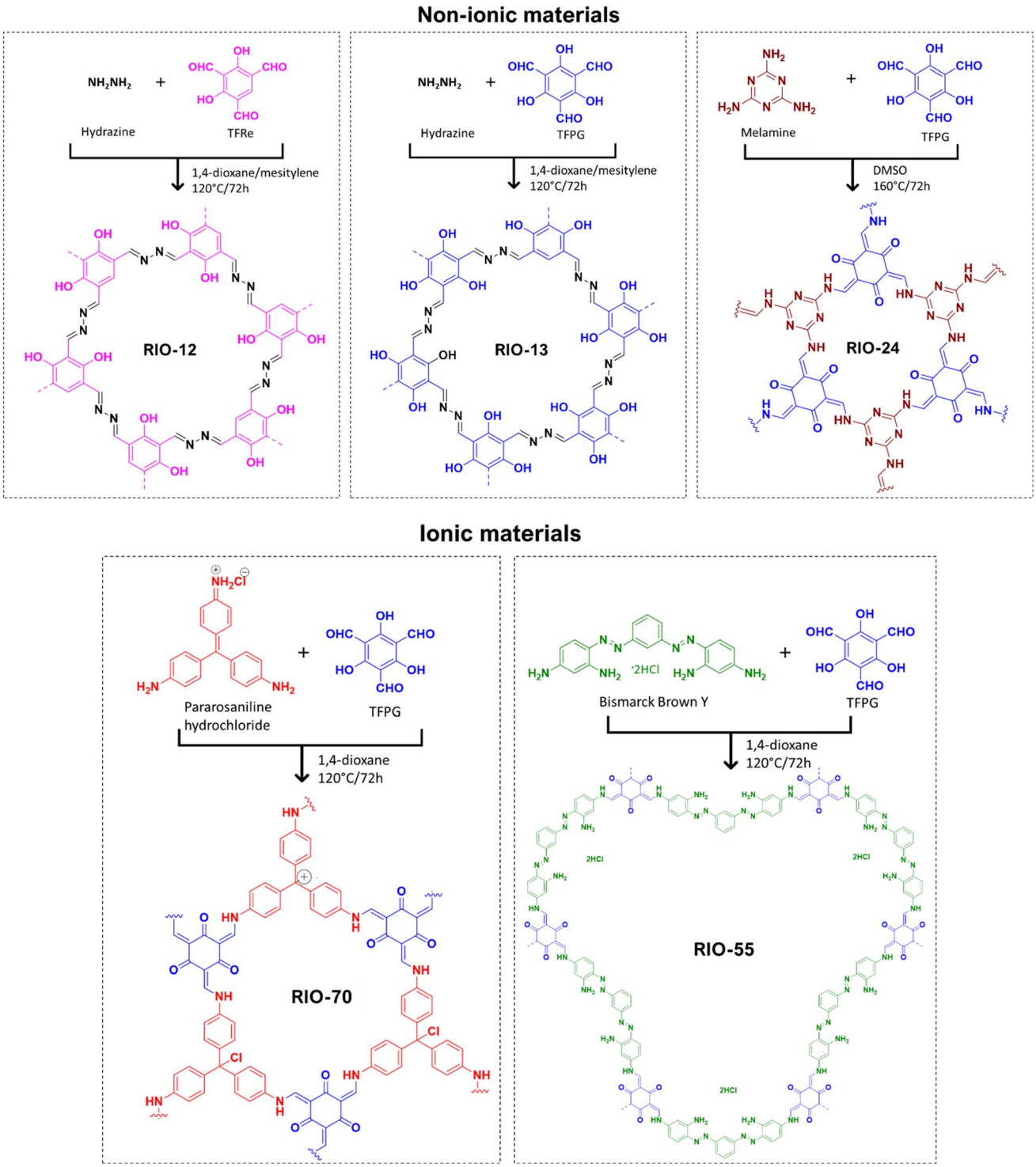

Fig. 2 The non-ionic and ionic nanoporous organic materials are used as adsorbents in this work.

30 min and then filtered and analysed by UV-vis. The adsorbent was retained on filter paper and then reused. For the desorption process, the materials were immersed in 70 mL of methanol under stirring (shaker) for 6 min. After this, the solution was filtered again and the solid remained in contact with new pollutant solutions. This process was carried out consecutively 4 times in the case of CLO and 3 times in the case of CIP.

Pollutant removal from a real water sample

Pollutant adsorption tests were performed on a real water sample, taken from the Tagus River in Portugal. First, the real sample was analysed by UV-vis to observe the adsorption bands present in the selected wavelength range (200–500 nm). When confirming the absence of absorption bands at 272 nm and

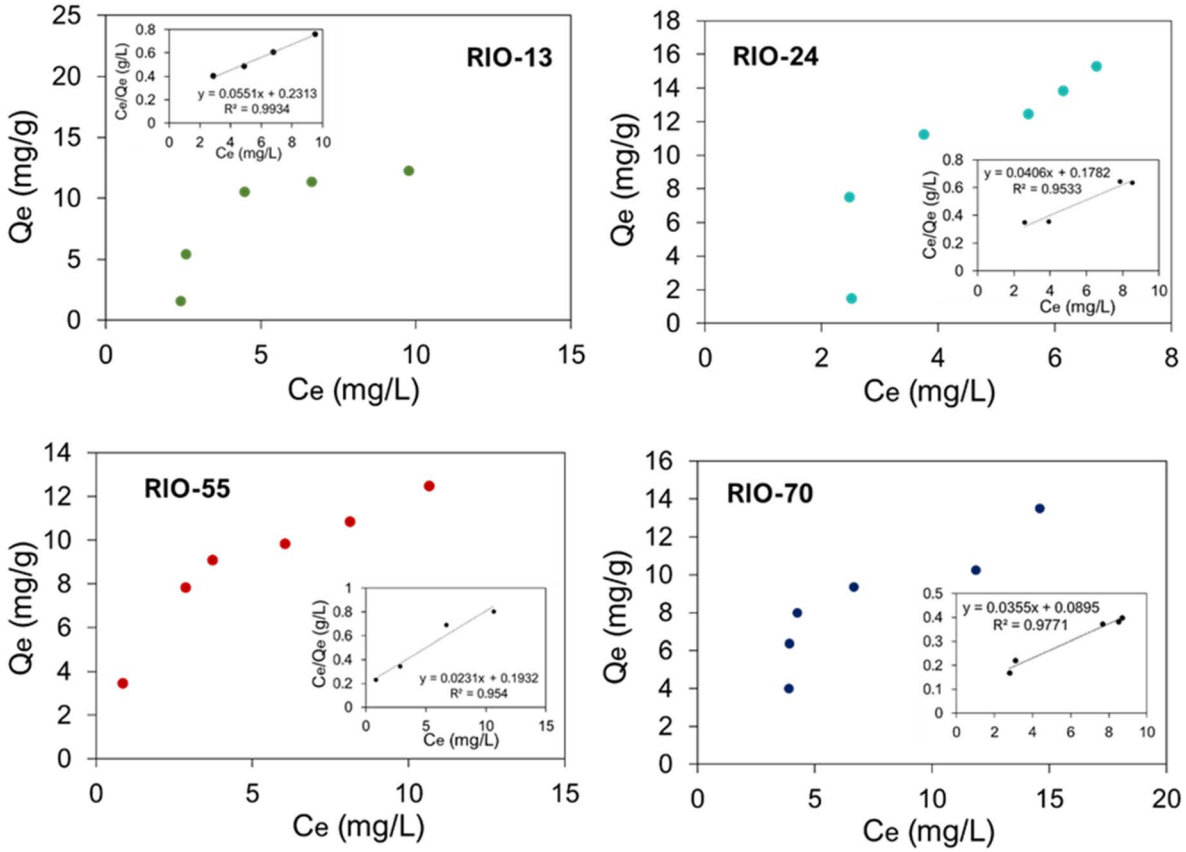

Fig. 3 Ciprofloxacin (CIP) adsorption isotherms (Langmuir model) and its non-linearized form (inset).

278 nm respectively (CIP and CLO), the solutions with the same concentrations as the tests described above were prepared. The calibration curves of the river water samples containing the same micropollutants were obtained by UV-vis spectroscopy as shown in Fig. S15 (ESI†). A good correlation was obtained for both cases ($R^2 > 0.99$). Thus, the antibiotics were included in the real sample. For the real assays, 4 mg of each adsorbent (**RIO-70** and **RIO-24**) was left in contact with 4 mL of pollutant solutions in a shaker for 24 h at 2400 rpm. After that, the solutions were filtered and analysed, as done under the previous conditions considering the same selected wavelength range (200–500 nm).

Results and discussion

The nanoporous adsorbents, RIOs, were selected according to their porosities and chemical structures including non-ionic (**RIO-12**, **RIO-13**, and **RIO-24**) and ionic (**RIO-55** and **RIO-70**) organic materials (Fig. 2). ^{13}C NMR of **RIO-24** exhibited an intense signal at ~166 ppm indicative of the triazine carbon. At ~184 ppm a C=O signal appears, showing the structure's preference for the keto-enamine form. However, a signal at ~54 ppm indicates that the structure is also formed for aminal-type bonds (N–CH–N). Probably, these connections must be pillaring the structure, which forms larger spaces, being detected as mesoporous (see Fig. S07†). The N_2 adsorption/desorption isotherm showed a hysteresis, typical of mesoporous materials, classified as type IV. The surface area obtained using the Brunauer–Emmett–Teller (BET) equation was 650 $m^2\ g^{-1}$, of which 248 $m^2\ g^{-1}$ refers to a microporous area and 402 $m^2\ g^{-1}$ to a mesoporous area, according to the calculated *t*-plot (De Boer). Pore size distribution indicated pores of 14 and 50 Å (see Fig. S07† inset). The PXRD for **RIO-24** presented

Table 1 Parameters from the Langmuir equation considering CLO and CIP removal and textural properties of the COFs

Ads	S_{BET} ($m^2\ g^{-1}$)	Q_{max} (mg g^{-1}) CIP	K_L CIP	Q_{max} (mg g^{-1}) CLO	K_L CLO
RIO-12	830	8.0	1.420	23.0	0.145
RIO-13	900	19.5	0.265	13.5	0.228
RIO-24	650	34.0	0.125	45.0	0.435
RIO-55	350	79.0	0.169	182.0	0.036
RIO-70	990	28.0	0.401	133.0	0.049

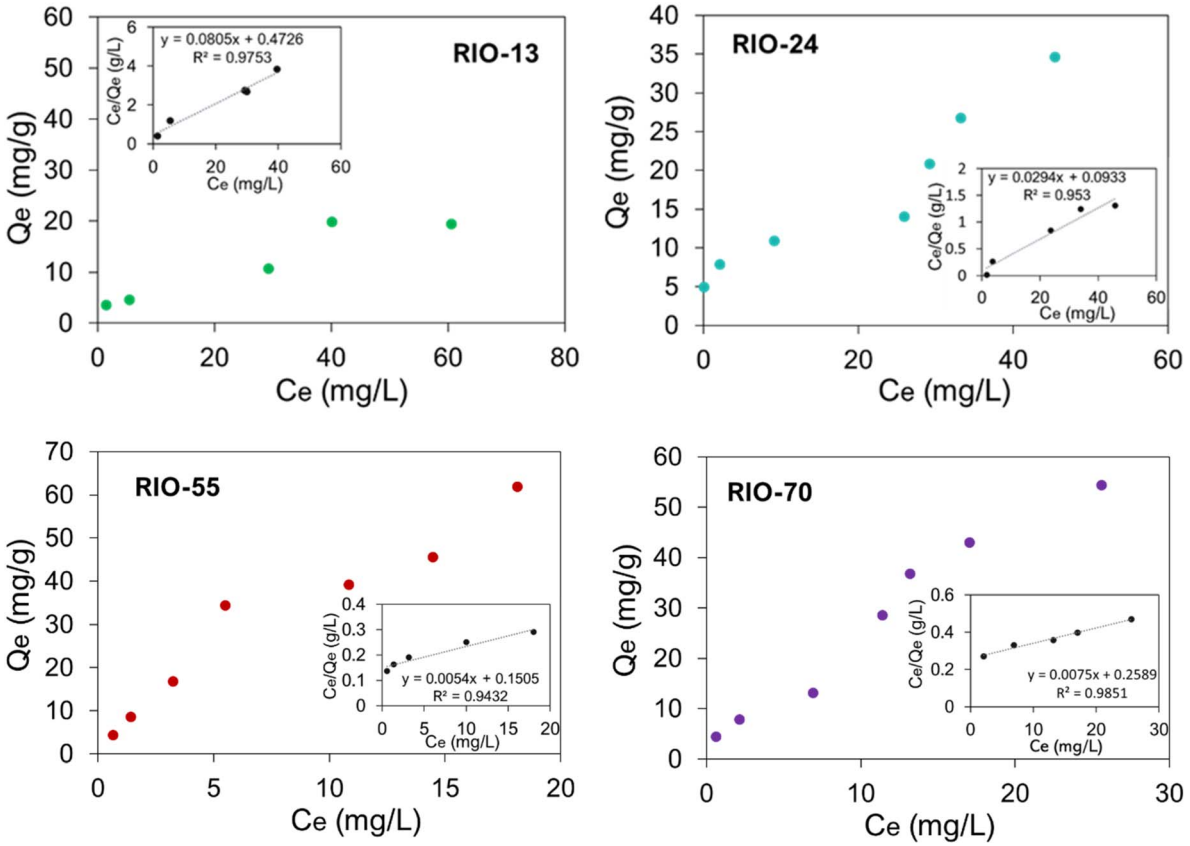

Fig. 4 Chloramphenicol (CLO) adsorption isotherms (Langmuir model) and its non-linearized form (inset).

low crystallinity possessing an intense peak at $\theta \sim 29°$ in agreement with forming a lamellar structure.

From the absorbance data obtained (see ESI, Fig. S14†), it was possible to find the final concentration values (C_e), according to the number of pollutants that have not been adsorbed by the RIOs. Therefore, the difference method ($C_i - C_e$) was applied to obtain the maximum adsorbed amount or adsorption capacity (Q_{max}). A Langmuir isotherm was generated for each of the adsorption processes, by plotting Q_e *versus* C_e. From its non-linearized form, the Q_{max} and K_L parameters were obtained, plotting C_e/Q_e *versus* C_e, according to the following equation:

$$\frac{C_e}{Q_e} = \frac{1}{Q_{max}} C_e + \frac{1}{K_L Q_{max}}$$

where C_e (mg L^{-1}) is the final concentration or concentration at equilibrium, Q_e (mg g^{-1}) is the amount of pollutant adsorbed at equilibrium, Q_{max} is the maximum adsorption capacity of the adsorbent at equilibrium (mg g^{-1}), and K_L is the constant interaction between the adsorbate and the adsorbent.

From the CLO and CIP calibration curves, the C_e values were adjusted according to the following equation:

$$C_e = (Abs_{initial} - b)/a$$

where the parameters a and b are obtained through the equation by plotting concentration *versus* absorbance, according to the Lambert–Beer law. The calibration curves obtained for CLO and CIP are in Fig. S13 (ESI†).

However, some isotherms were also plotted following Freundlich's theory. The equations and parameters suggested by this model are related to the heterogeneity of the adsorbents and the multilayers that can be formed in the pores and on the surface. Then, the linearized form of the Freundlich equations is:

$$\text{Log } Q_e = \log K_F + \frac{1}{n} \log C_e$$

where K_F is the Freundlich constant, representing the interception, and $1/n$ is the parameter correlated with the adsorption intensity, the slope, whose values can be attributed to stronger or weaker interactions between the adsorbates and adsorbent. If $n > 1$, this attraction is more relevant, presenting a great affinity and suggesting more favourable adsorption, while $1/n = n = 1$ indicates that both adsorption sites have the same energy (linear form).

Fig. 3 shows the Langmuir adsorption isotherms of CIP. The curves are classified as favourable, showing that the interaction between the adsorbent and adsorbate occurs as the concentration value increases, until equilibrium. The isotherms for **RIO-70**, **RIO-24**, and **RIO-13** are considered L-type (Langmuir), the most common for carbonaceous surfaces. On the other hand, **RIO-55** has an F-type isotherm, indicating some superficial heterogeneity. This classification is based on adsorption

processes on solids, where it is possible to see different surfaces in the same material and their levels of interaction with adsorbates.

The ionic and mesoporous **RIO-55** removed more CIP at room temperature. The values show that RIOs with larger pores such as **RIO-55** and **RIO-24** captured a greater amount of CIP due to the diffusion in the pores and on the surface. These diffusion steps occur in different ways, considering the size of the adsorbed molecules. It is important to note that this is a determining factor for microporous materials. In larger pores, molecules diffuse as if there were no pore walls. Table 1 shows the values of Q_{max} and K_L obtained from the Langmuir equation non-linearized for pollutant removal and the surface area (BET) and pore size of the adsorbents. Fig. 4 exhibits the Langmuir isotherms obtained for the adsorption of chloramphenicol (CLO) and its non-linearized form. As found for CIP, the CLO adsorption isotherms are of the favorable type, fitting with the Langmuir model, as the S (sigmoidal) type. However, the **RIO-70** isotherm shows a more favorable curve, with a less pronounced convex slope.

Using Freundlich's model, the linearized isotherms were obtained to determine the parameters and then be compared to the Langmuir ones. A summarized table was created to inform the obtained values for R^2 and $1/n$ for both models using all the RIOs and the antibiotics (see the ESI†). All the isotherms were of the favorable type (short values for $1/n$ and $n > 1$) following the assumptions of Freundlich's theory. These data coincide with the parameters found for the Langmuir model, presenting favorable adsorption. In this way, the preference or affinity of adsorbents with antibiotics, especially CLO, is observed.

Different adsorption mechanisms can occur during the process, such as the pore-size effect, π–π interaction, H-bonding, and hydrophobic interaction. As seen above, the pore size of RIOs is one of the determining factors for the capture of antibiotics. This is observed in situations where water is the fluid. There is also the contribution of hydrogen bonds, indicating greater adsorption of CLO than CIP, if we look at their structure. In addition, in the case of ionic materials, there are hydrophobic interactions due to the presence of charges. Therefore, **RIO-55** is more effective because of a set of factors that allow it to absorb more antibiotics.

For the ionic RIOs, the electrostatic interactions are more dominant, as commonly shown in published studies. However, the supporting interactions perform an important job in the

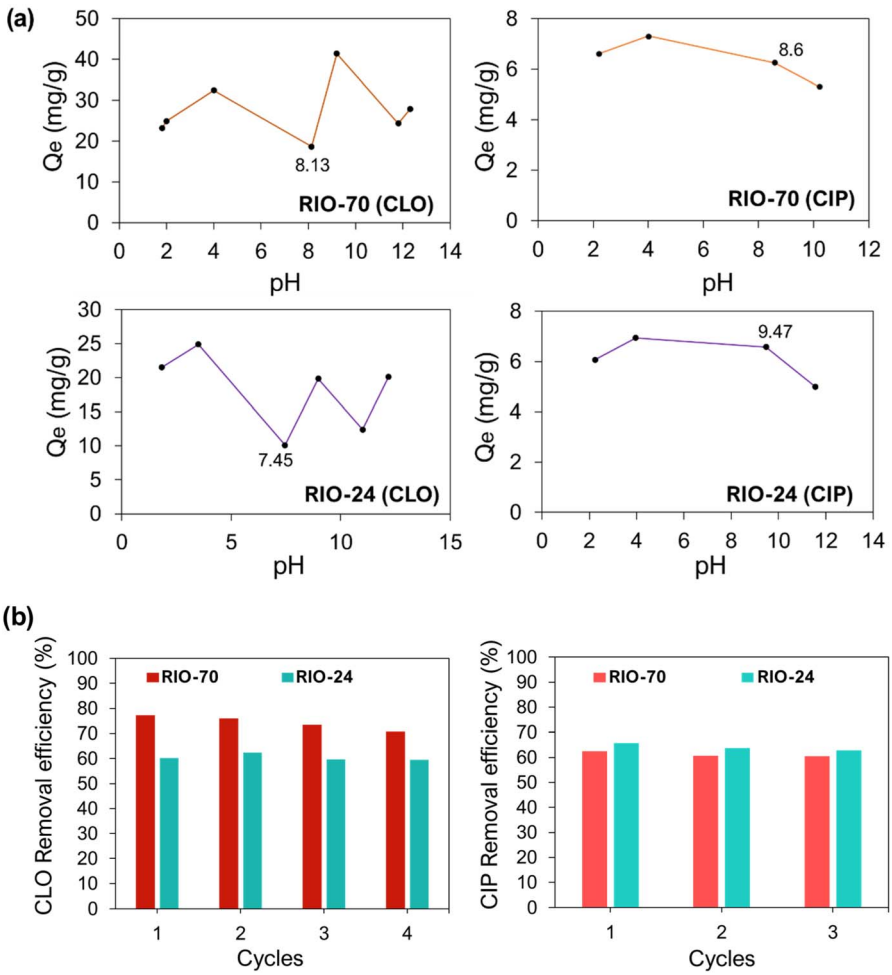

Fig. 5 (a) Adsorbed amount of CIP and CLO by **RIO-70** and **RIO-24** at different pHs; (b) regeneration cycles of **RIO-70** and **RIO-24** for CIP and CLO.

assembly. It is important to highlight that ciprofloxacin can exhibit different conformations, being easily ionized. This fact can contribute to more interactions between the RIOs and the antibiotic.

Besides this, the parameters applied from the Freundlich and Langmuir models show stronger interactions between the adsorbates and some COFs, mainly the ionic ones. Following Freundlich parameters, the values of $n > 2$ show that the adsorption intensity is greater in the ionic COFs than in the neutral. This suggests a strong intermolecular attraction between the solid and the adsorbates.

Some studies reported different materials as adsorbents for other organic pollutants, such as β-cyclodextrin COF[28] that captures 88 mg g^{-1} of bisphenol-A. Some commercial materials such as Brita AC and DARCO were used, capturing 19–24 mg g^{-1} of bisphenol-A. The porous material PDC-P captured 21 mg g^{-1} of bisphenol-S, 26 mg g^{-1} of propanol, and 22 mg g^{-1} of ethinyl estradiol. COF–NO_2 captured 70 mg g^{-1} of ketoprofen, 94 mg g^{-1} of ibuprofen, and 84 mg g^{-1} of naproxen.[29]

Adsorption tests with different pHs were performed for ciprofloxacin and chloramphenicol solutions, using **RIO-70** and **RIO-24** as adsorbents. Fig. 5a shows the adsorption behaviour and the Q_e values obtained for each pH. The pH of the chloramphenicol solution used in the **RIO-70** adsorption curves (*i.e.*, no acid or base added) was 8.13 and by **RIO-24**, the pH was 7.45. Observing the behaviour of the points in the figure, it is noticed that, at these pH values, there was the smallest adsorbed amount (Q_e), for both adsorbents. **RIO-70** adsorbed more of the CIP at a more basic pH (9.2), while **RIO-24** adsorbed better at an acidic pH (3.5).

The pH of the ciprofloxacin solution used in the adsorption tests with **RIO-70** was 8.59 while in the case of **RIO-24** it was 9.47. The adsorption values were not very discrepant with the pH change for ciprofloxacin, for both materials. The Q_e value is slightly better at more acidic pHs. It is also noted that the adsorption of chloramphenicol occurs faster when compared to ciprofloxacin. In about 30 min of contact (solution + adsorbent), the Q_e value for both RIOs is higher for chloramphenicol.

Pollutant removal efficiency tests were performed after several cycles. After the first adsorption of chloramphenicol on the adsorbents, another four cycles of adsorption were employed, using the same material filtered and treated with methanol. **RIO-70** lost more mass than **RIO-24** during the recycling process, due to the filtration step. Thus, only 4 to 5 cycles were performed for each material. Fig. 5b shows the number of cycles and the percentage of chloramphenicol and

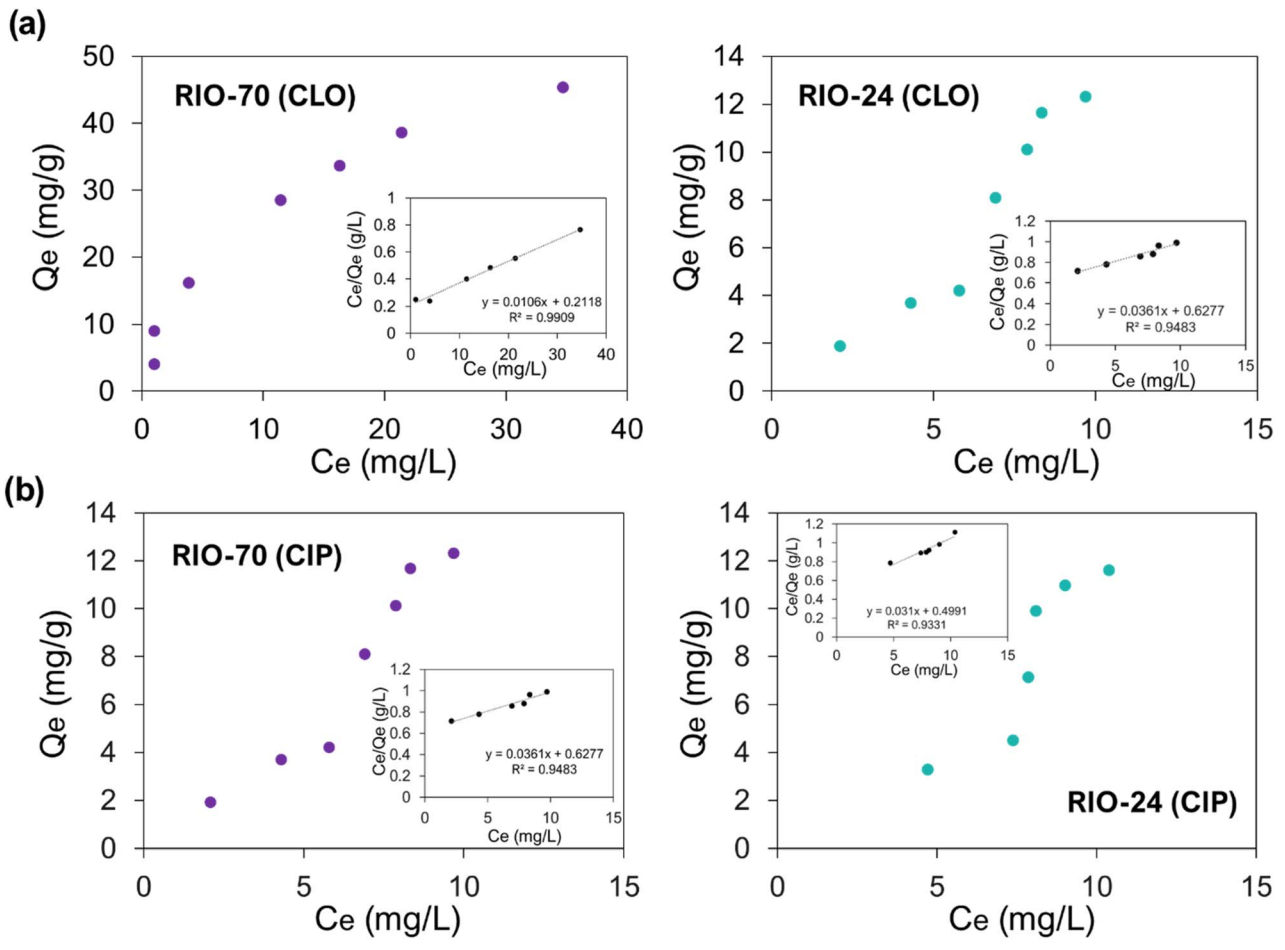

Fig. 6 (a) Adsorbed amount of CLO and (b) CIP by **RIO-70** and **RIO-24** in real water samples and their respective Langmuir non-linearized forms (inset).

ciprofloxacin adsorbed in each cycle. After 30 min of contact with CLO solution, **RIO-70** adsorbed about 70–80% of the pollutant, in an interval of 4 consecutive cycles. **RIO-24** captured about 60% of CLO during the 4 cycles. In the last cycle, there was a slight drop in the adsorption value by **RIO-70**, which may be due to the loss of mass during the filtration steps, which almost did not occur for **RIO-24**. For CIP, there are only 3 cycles in total, due to the type of paper used to filter the solutions (microfiber), which retained the material. Despite this, both adsorbents captured good amounts of the pollutant, maintaining the adsorption capacity in the 3 cycles.

In addition to performing adsorption tests using Milli-Q water, the efficiency of adsorbents in a real water sample was also tested. Fig. 6a shows the CLO and CIP adsorption isotherms of **RIO-70** and **RIO-24**. The Langmuir model was used, as well as its non-linearized form, from which the quantitative parameters (Q_{max} and K_L) were extracted. The obtained values of Q_{max} (CLO) for the real sample and Milli-Q water were very similar (133 mg g^{-1} for **RIO-70** and 25 mg g^{-1} for **RIO-24**). The CLO adsorption curve for **RIO-70** is L-type, proving to be highly favourable. Conversely, the **RIO-24** curve is S-type, but less favourable since it leans after remaining constant.

The CIP adsorption isotherms for **RIO-70** and **RIO-24** (Langmuir model) are S type, with a higher inclination for the **RIO-24** curve, whose convex region is more pronounced (Fig. 6b). The obtained Q_{max} values for both adsorbents in the real sample were practically the same compared to Milli-Q water (28 mg g^{-1} for **RIO-70** and 32 mg g^{-1} for **RIO-24**).

The similarity between the Q_{max} values found in the model tests and real water for the same pharmaceutical micropollutants shows the efficiency of removal by the adsorbents, in addition to proving to be selective for these compounds. The UV-vis spectra of the real sample exhibited an absorbance at ~200 nm, which decreased considerably after contact with the adsorbents. At ~350 nm, it was also possible to notice a less pronounced absorption band, which disappeared after adsorption (see the ESI† for more details).

Molecular interpretation

The data expressed in mass proportion (*i.e.*, mg g^{-1}) can be useful for engineering or practical reasons. However, for a better comprehension of the possible phenomenon, one should look at the number in (mol of API)/(mol of pores) to determine how many molecules of a given API can be included in the pore system. This enables the comparison of the performance of various COFs with different molecular masses per unit cell. Fig. 7 demonstrates, for instance, that the unit cell of **RIO-55** (blue), which has $C_{72}N_{24}H_{54}O_6$ and a molar mass (MW) of 1351.3866 g mol^{-1}, contains a single pore (yellow). That is valid for any COF with the same topology as **RIO-55**.

Thus, the molecular ratio of a given API per pore can be calculated as

$$\text{Loading per pore} = \frac{Q_{max}\ (\text{mg})/\text{MW}\ (\text{API})}{1\ \text{g}/\text{MW}\ (\text{unit cell})}$$

Table 2 shows the molar ratio of the APIs per pore for CLO and CIP and the pore size of the COF. It is noteworthy that **RIO-55** is the only COF that holds considerable amounts of API molecules in the pore system. This is related to its pore width since **RIO-55** has the largest pore system among the COFs studied. Actually one can observe a correlation between pore width of the COF and its ability to capture the API (Fig. 8).

Analysis of the geometries of the APIs and the pore systems of these COFs shows that only **RIO-55** can comfortably fit the APIs into its pore system, indicating that the other COFs may have diffusion problems for adsorbing them (Fig. 9).

Table 2 Molar ratio between the amount of API per pore for the COFs used in this study

		Unit cell of the COF		API per pore (mol mol^{-1})	
COF	Pore width (Å)	Formula	MW[a] (mol g^{-1})	CIP	CLO
RIO-12	11	$C_{18}N_6H_{12}O_4$	376.3333	0.01	0.03
RIO-13	11	$C_{18}N_6H_{12}O_6$	408.3321	0.02	0.02
RIO-24	8.8	$C_{12}N_6H_6O_3$	282.2196	0.03	0.04
RIO-55	34	$C_{72}N_{24}H_{54}O_6$	1351.3866	0.32	0.76
RIO-70	10	$C_{28}N_3H_{18}O_3Cl$	490.0047	0.05	0.20

[a] MW = molar mass of the unit cell.

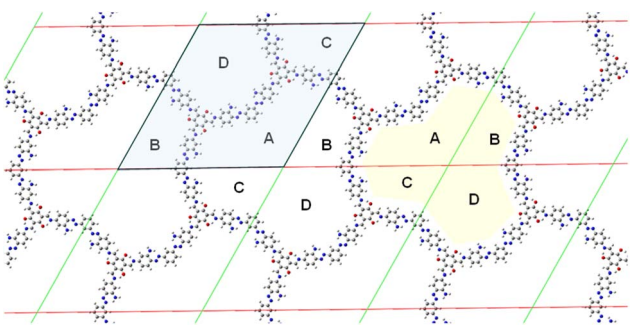

Fig. 7 Demonstration of the unit cell of RIO-55 forming a single pore.

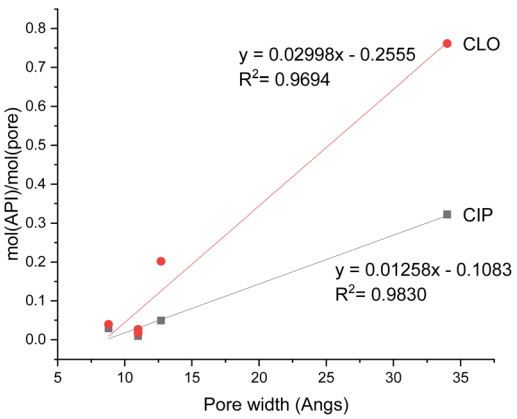

Fig. 8 Correlation of the loading of the API per pore (molar ratio) as a function of the pore width of the COF.

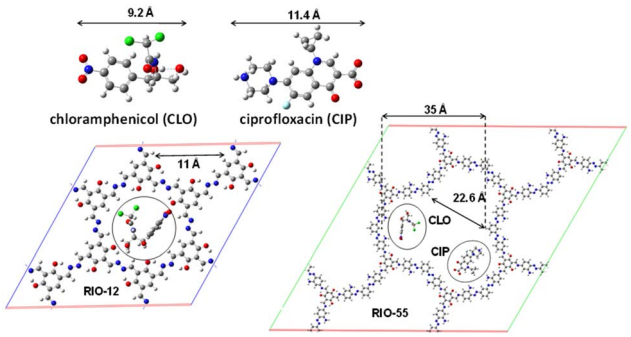

Fig. 9 Experimental geometries (X-rays) of the APIs and pore dimensions of RIO-12 (lower left) and RIO-55 (lower right), calculated from the quantum chemical level optimized structure at the DFT level.

Thus, it is plausible that mesoporous COFs are more suitable for the adsorption of APIs compared to microporous COFs. This can be a guideline for the design of new nanoporous materials for such a goal.

Conclusions

Ionic and non-ionic nanomaterials were pre-selected from their structural design and porosity to capture organic pollutants from water. For this, the antibiotics ciprofloxacin and chloramphenicol were chosen as adsorbates since they have increased occurrence in the water of rivers and seas. Generally, it was observed that materials with larger pores adsorb more pollutants. The removal efficiency is higher for materials composed of ionic structures, such as **RIO-55** and **RIO-70.** The strong interactions between the adsorbates and RIOs were determined using Langmuir and Freundlich parameters from linearized equations. These ionic materials can show more different ways of interaction, mainly electrostatic and hydrogen bonds. The Q_{max} values obtained for RIOs are higher in the literature for other organic pollutants. In addition, pH studies were performed, where the pollutant removal at different pHs varied considerably. RIOs can be regenerated at least 3 to 5 times, showing a good adsorption capacity, even after successive cycles of reuse. Finally, samples of real water from the Tagus River collected in Portugal were used to obtain the adsorption capacity of antibiotics using the selected materials, even competing with other molecules or existing fluids. The Q_{max} values obtained were similar or equal to those of the samples with pure water. RIOs presented better adsorption capacities than several adsorbents already reported. Indeed, this shows the good selectivity of these materials for CLO and CIP antibiotics and their removal efficiency. A correlation between the molar ratio of the maximum quantities of the APIs and the pore width of the COFs was observed. This shows that only **RIO-55** has enough space in its pore system to accommodate the APIs.

Data availability

The data supporting this article have been included as part of the ESI.†

Author contributions

The manuscript was written through the contributions of all authors. All authors have approved the final version of the manuscript. Sunny K. S. Freitas, Leticia R. C. Correa, and Verônica D. da Silva carried out the experiments and analysed the results. Luis C. Branco and Pierre M. Esteves formulated the concept of the project, planned the experiments, and managed the project.

Conflicts of interest

There are no conflicts to declare.

Acknowledgements

The authors acknowledge the CAPES, CNPq, FAPERJ, and FCT-MCTES for financial support and scholarships. Dr Fabio Henrique (UFRJ) is acknowledged for the computed geometries of the COFs at the DFT level. The authors also thank the following projects (PTDC/EAM-AMB/2023/2021 and 2022.07089.PTDC) funded by FCT.

References

1 W.-J. Ong, L.-L. Tan, Y. H. Ng, S.-T. Yong and S.-P. Chai, Graphitic Carbon Nitride (g-C_3N_4)-Based Photocatalysts for Artificial Photosynthesis and Environmental Remediation: Are We a Step Closer to Achieving Sustainability?, *Chem. Rev.*, 2016, **116**(12), 7159–7329, DOI: 10.1021/acs.chemrev.6b00075.

2 A. Alsbaiee, B. J. Smith, L. Xiao, Y. Ling, D. E. Helbling and W. R. Dichtel, Rapid Removal of Organic Micropollutants from Water by a Porous β-Cyclodextrin Polymer, *Nature*, 2015, **529**(7585), 190–194, DOI: 10.1038/nature16185.

3 Executive Agency for Health and Consumers, *Study on the Environmental Risks of Medicinal Products*, 2013.

4 J. P. R. d. Oliveira, *Estudo Dos Poluentes Orgânicos Persistentes (POPs) Em Regiões Industriais Da Grande São Paulo-via Cromatografia a Gás Acoplada a Espectrometria de Massas (GC-MS) e Captura de Elétrons (GC-ECD)*, 2011, pp. 1–182.

5 S. G. Akpe, I. Ahmed, P. Puthiaraj, K. Yu and W.-S. Ahn, Microporous Organic Polymers for Efficient Removal of Sulfamethoxazole from Aqueous Solutions, *Microporous Mesoporous Mater.*, 2020, **296**, 109979, DOI: 10.1016/j.micromeso.2019.109979.

6 Y. Li, J. Zhang and H. Liu, Removal of Chloramphenicol from Aqueous Solution Using Low-Cost Activated Carbon Prepared from Typha Orientalis, *Water*, 2018, **10**(4), 351, DOI: 10.3390/w10040351.

7 Y. Fan, B. Wang, S. Yuan, X. Wu, J. Chen and L. Wang, Adsorptive Removal of Chloramphenicol from Wastewater by NaOH Modified Bamboo Charcoal, *Bioresour. Technol.*, 2010, **101**(19), 7661–7664, DOI: 10.1016/j.biortech.2010.04.046.

8 Z. Xia, Y. Zhao and S. B. Darling, Covalent Organic Frameworks for Water Treatment, *Adv. Mater. Interfaces*, 2021, **8**(1), 1–17, DOI: **10.1002/admi.202001507**.

9 H. Fu, L. Gutierrez, S. Shewfelt, Y. Xiong and K. A. Gray, A Robust Self-Regenerating Graphene-Based Adsorbent for Pharmaceutical Removal in Various Water Environments, *Water Res.*, 2024, 121998, DOI: **10.1016/j.watres.2024.121998**.

10 D. Kanakaraju, B. D. Glass and M. Oelgemöller, Advanced Oxidation Process-Mediated Removal of Pharmaceuticals from Water: A Review, *J. Environ. Manage.*, 2018, 189–207, DOI: **10.1016/j.jenvman.2018.04.103**.

11 A. Paul, Water Treatment Using Chemically Activated Charcoal, *J. Sci. Technol.*, 2020, **5**(3), 72–78, DOI: **10.46243/jst.2020.v5.i3.pp72-78**.

12 R. Riaz, M. Ali, T. Maiyalagan, A. A. Arbab, A. S. Anjum, S. Lee, M. J. Ko and S. H. Jeong, Activated Charcoal and Reduced Graphene Sheets Composite Structure for Highly Electro-Catalytically Active Counter Electrode Material and Water Treatment, *Int. J. Hydrogen Energy*, 2020, **45**(13), 7751–7763, DOI: **10.1016/j.ijhydene.2019.06.138**.

13 Q. Sun, B. Aguila, J. Perman, L. D. Earl, C. W. Abney, Y. Cheng, H. Wei, N. Nguyen, L. Wojtas and S. Ma, Postsynthetically Modified Covalent Organic Frameworks for Efficient and Effective Mercury Removal, *J. Am. Chem. Soc.*, 2017, **139**(7), 2786–2793, DOI: **10.1021/jacs.6b12885**.

14 C.-H. Yang, J.-S. Chang and D.-J. Lee, Covalent Organic Framework EB-COF:Br as Adsorbent for Phosphorus (V) or Arsenic (V) Removal from Nearly Neutral Waters, *Chemosphere*, 2020, **253**, 126736.

15 S. K. S. Freitas, F. L. Oliveira, C. Merlini, E. P. S. Justo, A. Gioda and P. M. Esteves, Dye-Based Covalent Organic Networks (CONs), *J. Phys. Mater.*, 2020, **3**, 025011, DOI: **10.1088/2515-7639/ab854b**.

16 S. K. S. Freitas, F. L. Oliveira, T. C. Dos Santos, D. Hisse, C. Merlini, C. Machado and P. M. Esteves, A Carbocationic Triarylmethane-Based Porous Covalent Organic Network, *Chem.–Eur. J.*, 2020, **27**, 2342, DOI: **10.1002/chem.202003554**.

17 N. W. Ockwig, A. P. Co, M. O. Keeffe, A. J. Matzger and O. M. Yaghi, Porous, Crystalline, Covalent Organic Frameworks, *J. Phys. Mater.*, 2005, **310**, 1166–1171.

18 S. Chandra, S. Kandambeth, B. P. Biswal, B. Lukose, S. M. Kunjir, M. Chaudhary, R. Babarao, T. Heine and R. Banerjee, Chemically Stable Multilayered Covalent Organic Nanosheets from Covalent Organic Frameworks via Mechanical Delamination, *J. Am. Chem. Soc.*, 2013, **135**(47), 17853–17861, DOI: **10.1021/ja408121p**.

19 Z. Xiang, S. An, Y. Liu, J. Hu and H. Liu, Efficient Removal of Organic Dyw Pollutants Using Covalent Organic Frameworks, *American Institute of Chemical Engineers Journal*, 2017, **61**(3), 1–15, DOI: **10.1002/aic**.

20 W. Guo, J. Liu, H. Tao, J. Meng, J. Yang, Q. Shuai, Y. Asakura, L. Huang and Y. Yamauchi, Covalent Organic Framework Nanoarchitectonics: Recent Advances for Precious Metal Recovery, *Adv. Mater.*, 2024, **36**(33), DOI: **10.1002/adma.202405399**.

21 H. Tao, W. Guo, J. Liu, Y. Shi, H. Tao, Q. Shuai and L. Huang, Deciphering the Relationship between the Ordered Pore Structure and Solid-Phase Microextraction Behavior of Covalent Organic Frameworks for Phenols, *J. Hazard. Mater.*, 2024, **467**, 133764, DOI: **10.1016/j.jhazmat.2024.133764**.

22 H. Da, C. Yang and X. Yan, Cationic Covalent Organic Nanosheets for Rapid and Selective Capture of Perrhenate: An Analogue of Radioactive Pertechnetate from Aqueous Solution, *Environ. Sci. Technol.*, 2019, **53**(9), 5212–5220, DOI: **10.1021/acs.est.8b06244**.

23 O. M. Yaghi, M. J. Kalmutzki and C. S. Diercks, *Introduction to Reticular Chemistry*, Wiley-VCH Verlag GmbH & Co. KGaA, 2019, DOI: **10.1002/9783527821099**.

24 R. A. Maia, F. Lopes Oliveira, V. Ritleng, Q. Wang, B. Louis and P. Mothé Esteves, CO_2 Capture by Hydroxylated Azine-Based Covalent Organic Frameworks, *Chem.–Eur. J.*, 2021, **27**(30), 8048–8055, DOI: **10.1002/chem.202100478**.

25 R. A. Maia, F. L. Oliveira, M. Nazarkovsky and P. M. Esteves, Crystal Engineering of Covalent Organic Frameworks Based on Hydrazine and Hydroxy-1,3,5-Triformylbenzenes, *Cryst. Growth Des.*, 2018, **18**, 5682–5689.

26 S. K. S. Freitas, F. L. Oliveira, T. C. Dos Santos, D. Hisse, C. Merlini, C. Machado and P. M. Esteves, A Carbocationic Triarylmethane-Based Porous Covalent Organic Network, *Chem.–Eur. J.*, 2021, **27**(7), 2342–2347, DOI: **10.1002/chem.202003554**.

27 R. A. Maia, F. L. Oliveira, M. Nazarkovsky and P. M. Esteves, Crystal Engineering of Covalent Organic Frameworks Based on Hydrazine and Hydroxy-1,3,5-Triformylbenzenes, *Cryst. Growth Des.*, 2018, **18**(9), 5682–5689, DOI: **10.1021/acs.cgd.8b01110**.

28 A. Alsbaiee, B. J. Smith, L. Xiao, Y. Ling, D. E. Helbling and W. R. Dichtel, Rapid Removal of Organic Micropollutants from Water by a Porous β-Cyclodextrin Polymer, *Nature*, 2015, **529**(7585), 190–194, DOI: **10.1038/nature16185**.

29 Y. Liang, L. Feng, X. Liu, Y. Zhao, Q. Chen, Z. Sui and N. Wang, Enhanced Selective Adsorption of NSAIDs by Covalent Organic Frameworks via Functional Group Tuning, *Chem. Eng. J.*, 2021, **404**, 127095, DOI: **10.1016/j.cej.2020.127095**.